

## 1 Ultrafast Intramolecular Exciton Splitting Dynamics in Isolated Low- 2 Band-Gap Polymers and Their Implications in Photovoltaic Materials 3 Design

4 Brian S. Rolczynski,<sup>†,‡,§</sup> Jodi M. Szarko,<sup>†,‡,§</sup> Hae Jung Son,<sup>‡,||</sup> Yongye Liang,<sup>||</sup> Luping Yu,<sup>\*,‡,||</sup>  
5 and Lin X. Chen<sup>\*,†,‡,§</sup>

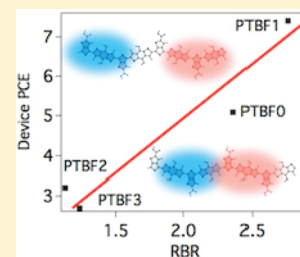
6 <sup>†</sup>Department of Chemistry and <sup>‡</sup>ANSER Center, Northwestern University, 2145 Sheridan Road, Evanston, Illinois 60208, United  
7 States

8 <sup>§</sup>Chemical Sciences and Engineering Division, Argonne National Laboratory, 9700 South Cass Avenue, Argonne, Illinois, 60439,  
9 United States

10 <sup>||</sup>Department of Chemistry and The James Franck Institute, The University of Chicago, 929 East 57th Street, Chicago, Illinois 60637,  
11 United States

### 12 **S** Supporting Information

13 **ABSTRACT:** Record-setting organic photovoltaic cells with PTB polymers have recently  
14 achieved ~8% power conversion efficiencies (PCE). A subset of these polymers, the PTBF series,  
15 has a common conjugated backbone with alternating thieno[3,4-*b*]thiophene and benzodithio-  
16 phene moieties but differs by the number and position of pendant fluorine atoms attached to the  
17 backbone. These electron-withdrawing pendant fluorine atoms fine tune the energetics of the  
18 polymers and result in device PCE variations of 2–8%. Using near-IR, ultrafast optical transient  
19 absorption (TA) spectroscopy combined with steady-state electrochemical methods we were able  
20 to obtain TA signatures not only for the exciton and charge-separated states but also for an  
21 intramolecular (“pseudo”) charge-transfer state in isolated PTBF polymers in solution, in the  
22 absence of the acceptor phenyl-C<sub>61</sub>-butyric acid methyl ester (PCBM) molecules. This led to the  
23 discovery of branched pathways for intramolecular, ultrafast exciton splitting to populate (a) the charge-separated states or (b)  
24 the intramolecular charge-transfer states on the time scale of subpicoseconds to a few nanoseconds. Depending on the number  
25 and position of the fluorine pendant atoms, the charge-separation/transfer kinetics and their branching ratios vary according to  
26 the trend for the electron density distribution in favor of the local charge-separation direction. More importantly, a linear  
27 correlation is found between the branching ratio of intramolecular charge transfer and the charge separation of hole–electron  
28 pairs in isolated polymers versus the device fill factor and PCE. The origin of this correlation and its implications in materials  
29 design and device performance are discussed.



## 1. INTRODUCTION

30 Conjugated alternating copolymers, in which conjugated blocks  
31 with different electron affinities are alternately arranged in  
32 sequence along the polymer backbone, have recently shown  
33 relatively high power conversion efficiencies (PCEs) of >8% in  
34 bulk heterojunction (BHJ) organic photovoltaic (OPV)  
35 devices.<sup>1–3</sup> These higher PCEs, relative to those from  
36 benchmark homopolymers such as poly(3-hexylthiophene)  
37 (P3HT), are attributed in part to more efficient solar photon  
38 harvesting in the near-infrared (NIR) region due to a lower  
39 optical gap. Extensive studies on P3HT and its derivatives have  
40 rendered a wealth of information about the importance of the  
41 following factors upon device PCE: polymer regioregularity and  
42 conjugation length,<sup>4–6</sup> film morphology,<sup>7,8</sup> crystallinity,<sup>9</sup>  
43 molecular orientation,<sup>10,11</sup> charge carrier mobilities,<sup>12–14</sup> light  
44 harvesting efficiency in the solar spectrum,<sup>15</sup> and device  
45 fabrication conditions.<sup>16,17</sup> However, correlations between  
46 device performance and intrinsic properties of polymers,  
47 including structure, energetics, and charge carrier/exciton  
48 dynamics, remain unclear. In particular, the ultrafast exciton

splitting and charge carrier dynamics of the *isolated* donor  
polymers *in solution* have not been correlated directly to the  
device PCE because (a) a large number of parallel and  
sequential processes on both ultrafast and slow time scales  
occur only in device-relevant conditions and (b) only exciton  
splitting at the donor–acceptor BHJs is believed to determine  
the overall device PCE. It is commonly known that excitons  
split at donor–acceptor BHJs much faster and more efficiently  
than they do via intramolecular processes.<sup>18</sup> The LUMO energy  
level offset of the polymer and the PCBM has been used to  
estimate the driving force requirement for the exciton splitting,  
but even this picture is inaccurate because it neglects the energy  
level modifications due to the BHJ. Since there is no apparent  
BHJ of isolated polymers in solution, there is no reason to  
expect that the polymer alone should have exciton dynamics  
relevant to the device. Therefore, optimization of donor  
polymers has been carried out largely upon the energetics via

Received: September 24, 2011

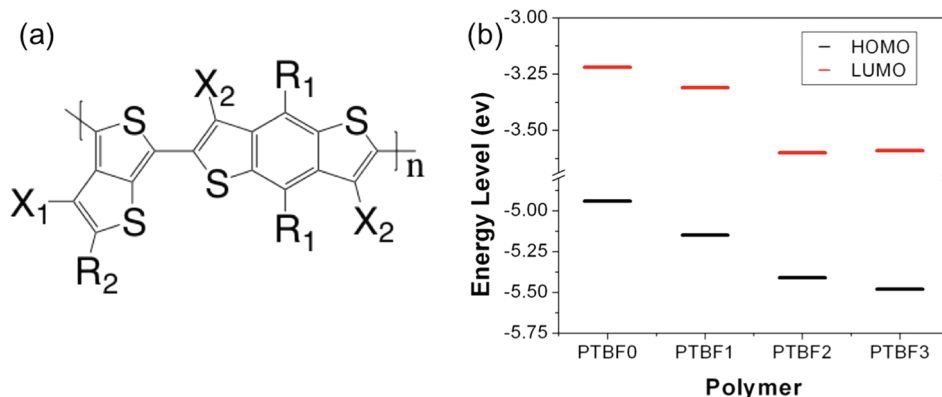


**Figure 1.** (a) PTBF series structure.  $R_1$  is octyloxy for PTBF0 and octyloxy(2-ethylhexyl) for PTBF1, PTBF2, and PTBF3.  $R_2$  is 2-ethylhexyl ester for all polymers.  $X_1$  is F for PTBF1 and PTBF2 and H otherwise.  $X_2$  is F for PTBF2 and PTBF3 and H otherwise. (b) HOMO and LUMO levels for the PTBF series as reported previously.<sup>17,26</sup>

66 tuning the ground and lowest singlet excited states of the  
 67 polymer with respect to those of the electron acceptor,  
 68 commonly phenyl- $C_{60}$ -butyric acid methyl ester (PCBM). For  
 69 instance, recent research and development of OPV materials  
 70 have yielded various new conjugated polymers<sup>18–23</sup> designed to  
 71 (a) raise the PCE by achieving a higher open-circuit voltage  
 72 ( $V_{OC}$ )<sup>24,25</sup> through lowering the polymer HOMO energy with  
 73 respect to the LUMO of the PCBM and (b) extend the spectral  
 74 overlap of the polymer absorption with the solar spectrum by  
 75 decreasing the polymer's optical gap. Two closely related sets of  
 76 these polymers have recently been synthesized, the PTB and  
 77 PTBF series, which are composed of alternating, regioregular  
 78 benzodithiophene (BDT) and thienothiophene (TT) moieties  
 79 (Figure 1), where the electron affinity is higher in the TT.<sup>11,19</sup>

80 The PTB series was originally developed by variation of the R  
 81 and  $X_1$  positions, whereas the PTBF series was later developed  
 82 by systematic fluorination at the  $X_1$  and  $X_2$  positions along the  
 83 polymer fragment (Figure 1). The studies reported here are  
 84 conducted on four polymers in the PTBF series, one of which  
 85 was the first polymer to exhibit a high PCE (7.4%) in devices,  
 86 while the PCE of the other polymers were 5.1%, 3.2%, and  
 87 2.7% for PTBF0, PTBF2, and PTBF3, respectively.<sup>1,18,26</sup>

88 Because the chemical structural differences in the PTBF  
 89 series are minor, it is important to investigate what causes such  
 90 significant variations in device PCE within this series of  
 91 copolymers with similar molecular packing characteristics<sup>11</sup> and  
 92 energetics.<sup>1,18,26</sup> This study highlights the importance of the  
 93 intrinsic properties of alternating copolymers at a molecular  
 94 level to the BHJ devices. In this report, we will demonstrate  
 95 that these alternating copolymers in fact are not just p-type  
 96 semiconductors acting as electron sources; they have intra-  
 97 molecular, ultrafast exciton splitting dynamics of their own and  
 98 are capable of generating charge-transfer or charge-separated  
 99 populations on a subpicosecond time scale. More interestingly,  
 100 we observed that these polymers' intrinsic dynamic properties  
 101 are closely correlated with device performance in BHJ films in  
 102 the presence of the electron acceptor PCBM. This study  
 103 searches for answers to the following questions: (a) how do the  
 104 intramolecular exciton splitting dynamics depend on the  
 105 moieties that make up the conjugated backbone, (b) what is  
 106 the driving force for intramolecular charge separation, and (c)  
 107 how are the intrinsic exciton splitting dynamics correlated with  
 108 BHJ device parameters, such as fill factor (FF) and PCE?<sup>27</sup>  
 109 Moreover, we will search for implications of these correlations

in materials design and OPV device optimization as well as  
 long-term development of solar cell market viability.

## 2. EXPERIMENTAL AND COMPUTATIONAL METHODS

**2.1. Sample Preparation.** PTBF0, PTBF1, PTBF2, and PTBF3  
 (Figure 1) were synthesized according to a previously reported  
 procedure.<sup>18,26</sup> Experimental details regarding the bulk device  
 characteristics, such as  $I$ - $V$  curves,  $J_{sc}$ ,  $V_{oc}$ , FF, PCE, and polymer  
 HOMO and LUMO energies, are also found in these sources. Solution  
 samples were prepared in chlorobenzene (CB).

**2.2. Steady-State Absorption.** Steady-state absorption spectra  
 (Figure 2) of solution and films were taken using a UV-3600 UV-vis-  
 NIR spectrophotometer (Shimadzu, Columbia, MD).

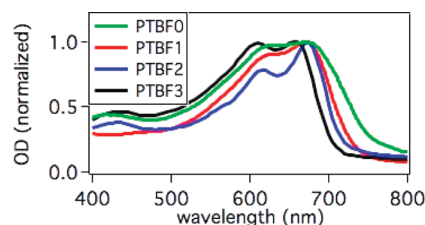


**Figure 2.** Normalized ground-state absorption spectra for the PTBF polymers.

To verify the polymer cation absorption features in solution, 121  
 absorption spectra of the chemically oxidized polymer cation were 122  
 measured in a spectral region of 200–1600 nm after titrating the 123  
 solution samples with  $FeCl_3$  (Aldrich). The chemically oxidized cation 124  
 spectra were extracted by subtracting the spectra of the same solution 125  
 prior to addition of  $FeCl_3$  (see the Supporting Information). 126

**2.3. Electronic Structure Calculations.** Calculations were 127  
 performed on model oligomers of corresponding PTBF polymers 128  
 using the HyperChem software package (Hypercube, Inc., Gainesville, 129  
 FL). Geometry optimizations of the oligomers with truncated aliphatic 130  
 side chains were initiated using the AM1 parametrization. Calculations 131  
 were subsequently carried out by the ZINDO/S method on both 132  
 asymmetric (BDT-TT)<sub>4</sub> and symmetric TT-(BDT-TT)<sub>4</sub> tetramers. 133  
 Configuration interaction (CI) calculations were performed using 20 134  
 orbitals above the HOMO and below the HOMO and LUMO gap. 135

**2.4. Transient Absorption Spectroscopy.** Transient absorption 136  
 (TA) spectra were measured using an ultrafast laser system by Spectra- 137  
 Physics at the Center for Nanoscale Materials in Argonne National 138  
 Laboratory. A 600 nm pump beam at 1.67 kHz was generated by an 139  
 optical parametric amplifier system (TOPAS, Light Conversion Ltd.) 140  
 and pumped by a regenerative amplifier (Spitfire Pro, Spectra Physics 141  
 Lasers) operating at a 5 kHz repetition rate. The Spitfire Pro was 142  
 pumped by an Nd:YLF laser (Empower, Spectra-Physics Lasers) and 143

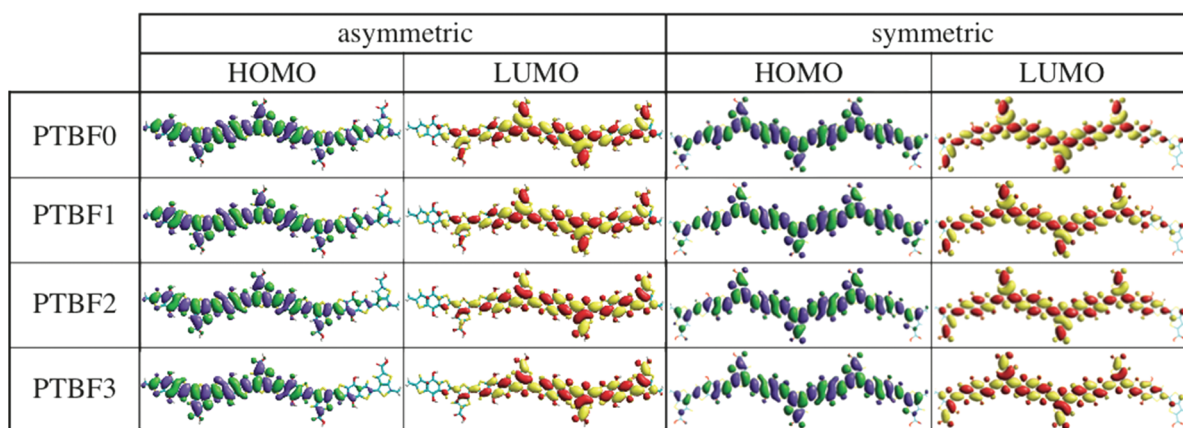


Figure 3. HOMO and LUMO for PTBF-like  $(\text{BDT-TT})_4$  (left) and  $\text{TT}(\text{BDT-TT})_4$  (right) tetramers. Side chains are truncated for clarity.

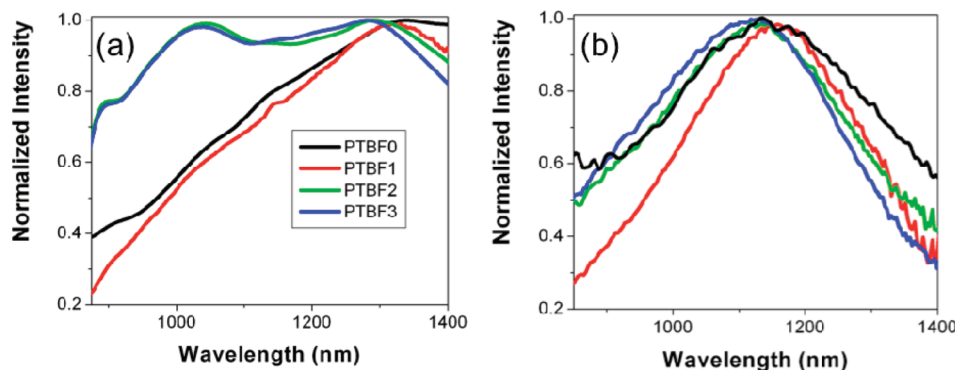


Figure 4. Normalized transient absorption spectra for the PTBF polymers at 2 ps (a) and 2.5 ns (b) pump–probe delay times. Excitation wavelength is 600 nm.

144 seeded by a Ti:sapphire oscillator (Tsunami, Spectra-Physics Lasers)  
 145 that was pumped by a Nd:YVO<sub>4</sub> laser (Millennia, Spectra Physics  
 146 Lasers). The output beam of the amplifier laser was split off and  
 147 chopped at 833 Hz. These beams were used to pump a TA  
 148 spectrometer (HELIOS, Ultrafast Systems LLC). A white light/NIR  
 149 probe was generated by focusing the 800 nm beam into a sapphire  
 150 plate. The 800–1500 nm component of this probe light was collected  
 151 by a CCD device. The detection spectral region is 850–1400 nm.  
 152 Samples were pumped at 600 nm using a focused 100  $\mu\text{m}$  diameter, 20  
 153 nJ/pulse. The cuvette path length was 2 mm, and the instrument  
 154 response function (IRF) was 160 fs fwhm. NIR TA spectra were  
 155 generated as two-dimensional data sets along time and wavelength  
 156 axes.

### 3. RESULTS

157 **3.1. Calculated Electronic Structures.** PTBF0, PTBF1,  
 158 PTBF2, and PTBF3 were modeled by their corresponding  
 159  $(\text{BDT-TT})_4$  oligomers with energy-minimized structures using  
 160 the AM1 method. The HOMO and LUMO for each species are  
 161 shown in Figure 3. Calculations for the tetramers correspond-  
 162 ing to PTBF0, PTBF1, PTBF2, and PTBF3 converged to  
 163 binding energies of  $-270$ ,  $-278$ ,  $-285$ , and  $-292$  MJ/mol,  
 164 respectively, indicating a trend of lowering the energy via the  
 165 number of pendant fluorines.

166 The CI calculations on model  $(\text{BDT-TT})_4$  oligomers suggest  
 167 that the lowest energy absorption band corresponds to mostly a  
 168 HOMO–LUMO transition. The electron density distributions  
 169 of HOMOs in these oligomers are more concentrated toward  
 170 the BDT end, while those of LUMOs are more concentrated  
 171 toward the TT end. Therefore, the HOMO–LUMO transition  
 172 creates a net electron density shift from one segment of the

173 oligomer to the other segment, reminiscent of the charge  
 174 separation in covalently linked donor–acceptor supermolecules  
 175 in the literature.<sup>28</sup> When an additional TT unit is attached to  
 176  $(\text{BDT-TT})_4$  to form a central symmetric  $\text{TT}(\text{BDT-TT})_4$   
 177 sequence (Figure 3), the HOMOs and LUMOs show a more  
 178 evenly distributed electron density across the oligomers and the  
 179 electron density shift due to the HOMO–LUMO transition is  
 180 less pronounced compared to that in  $(\text{BDT-TT})_4$  oligomers.  
 181 The dipole moments of the corresponding BDT-TT monomer  
 182 segments were also calculated and are shown in the Supporting  
 183 Information.

184 **3.2. Transient Absorption (TA) Spectra and Dynamics.**  
 185 Normalized TA spectra of the PTBF polymers 2 ps after  
 186 excitation by 600 nm light are shown in Figure 4a. These TA  
 187 spectra are broad across the 900–1400 nm region but differ  
 188 most strikingly near 1000 nm, where higher TA signals were  
 189 found when the BDT moiety was fluorinated (PTBF2 and  
 190 PTBF3). Kinetic traces taken in the 1350 nm region largely  
 191 decay within 700–1000 ps, while those in the 950 nm region  
 192 largely decay within 500–600 ps (Supporting Information).  
 193 After these components decayed, a Gaussian-shaped feature at  
 194 approximately 1150 nm remained. The normalized TA spectra  
 195 of these polymers at 3 ns delay time (Figure 4b) show a single  
 196 peak centered in the 1140–1160 nm region. Therefore, the  
 197 time evolution of the TA spectra for the four polymers suggests  
 198 the population of multiple states soon after excitation. Detailed  
 199 analyses indicated that these TA spectra can be best  
 200 approximated by three distinct Gaussian functions with their  
 201 central positions at approximately 1000, 1150, and 1350 nm  
 202 (see the Supporting Information).

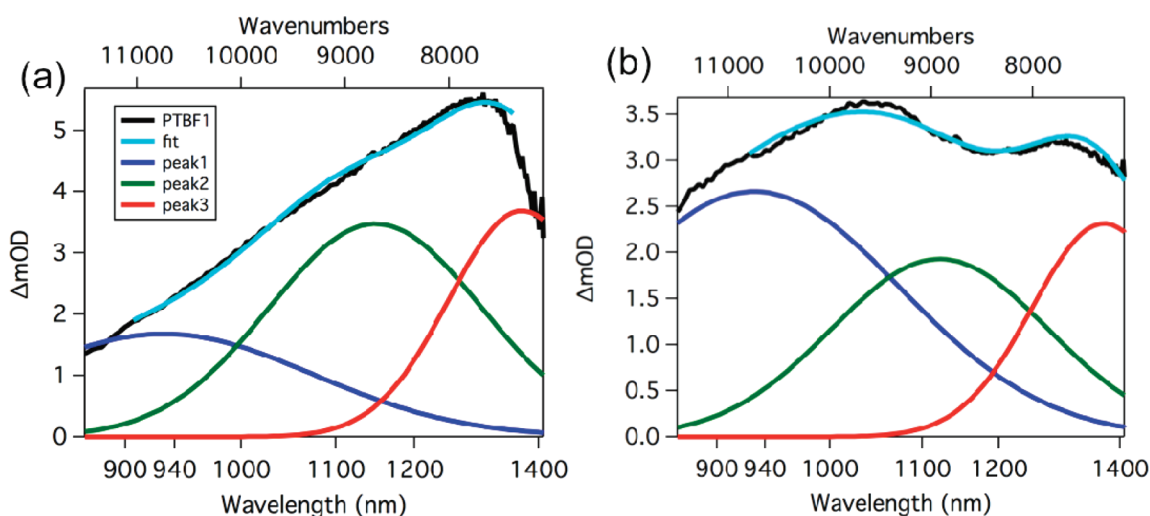


**Figure 5.** Transient absorption spectral fits of PTBF1 (a) and PTBF2 (b) at a delay time of 2 ps. This is an example of the spectral fit performed using a three-Gaussian fitting method (Supporting Information). Light blue curve is the sum of the three Gaussian curves representing the three spectral features identified in the spectrum, colored blue, green, and red.

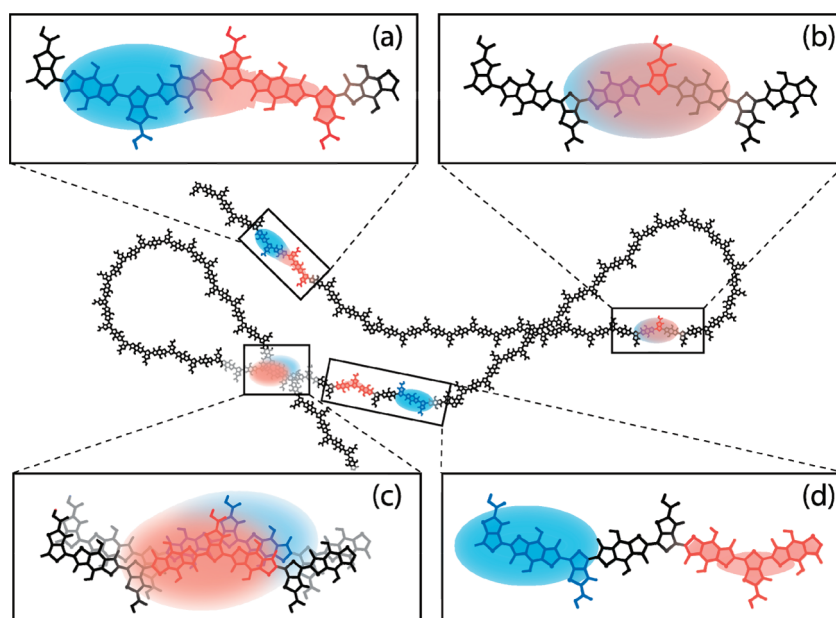


**Figure 6.** Illustration for delocalized electrons (red) and holes (blue) in intrachain PCT (a), EX (b), interchain PCT (c), and CS (d) states of an isolated polymer in solution.

fs 203 The TA spectra of PTBF1 and PTBF2 are shown in Figure  
 fs 204 5, along with the fits of the spectra using the three-component  
 205 analysis (see the Supporting Information for details). The TA  
 206 spectral feature at approximately 1150 nm is assigned to the  
 207 polymer cation absorption. This assignment is based on two  
 208 experimental observations. First, this signal coincides with the  
 209 cation TA feature in the corresponding BHJ films with the  
 210 same polymers and PCBM, where the charge separation is  
 211 efficient and long lasting (the Supporting Information).<sup>10</sup>  
 212 Second, this signal closely resembles the polymer cation  
 213 features in the steady-state absorption spectrum after adding  
 214 an oxidant FeCl<sub>3</sub> into the solution (see the Supporting  
 215 Information).

216 The broad TA feature around 1350 nm is assigned to the  
 217 exciton (EX) state absorption for the following reasons. First,  
 218 its lifetime agrees with other exciton lifetimes of 500–1000 ps  
 219 in isolated polymers in the literature<sup>29</sup> and is much shorter than

the lifetime of the cation signal, which has a time constant of 220  
 longer than a few nanoseconds. Second, it corresponds well to a 221  
 TA feature in the same spectral region in the BHJ film (Figures 222  
 S4 and S5 in the Supporting Information), whose decay 223  
 corresponds well to the rise of the cation TA signal due to the 224  
 EX-to-charge-separated (CS) state conversion. If the exciton- 225  
 splitting process were slow, then the TA spectrum at early delay 226  
 times would be almost entirely from the EX state as in 227  
 previously studied conjugated homopolymers in solution<sup>29</sup> and 228  
 the assignment would be straightforward. However, we 229  
 observed evidence of subpicosecond generation of other states 230  
 (to be described in detail later), so the earliest TA spectrum 231  
 cannot be assigned solely to the EX state signal. The main 232  
 interfering species at the early delay time is the cation, with its 233  
 broad feature centered around 1150 nm, while the other feature 234  
 around 1000 nm has much less influence on the EX signal. 235  
 Hence, we subtracted a scaled TA spectrum at 3 ns delay from 236

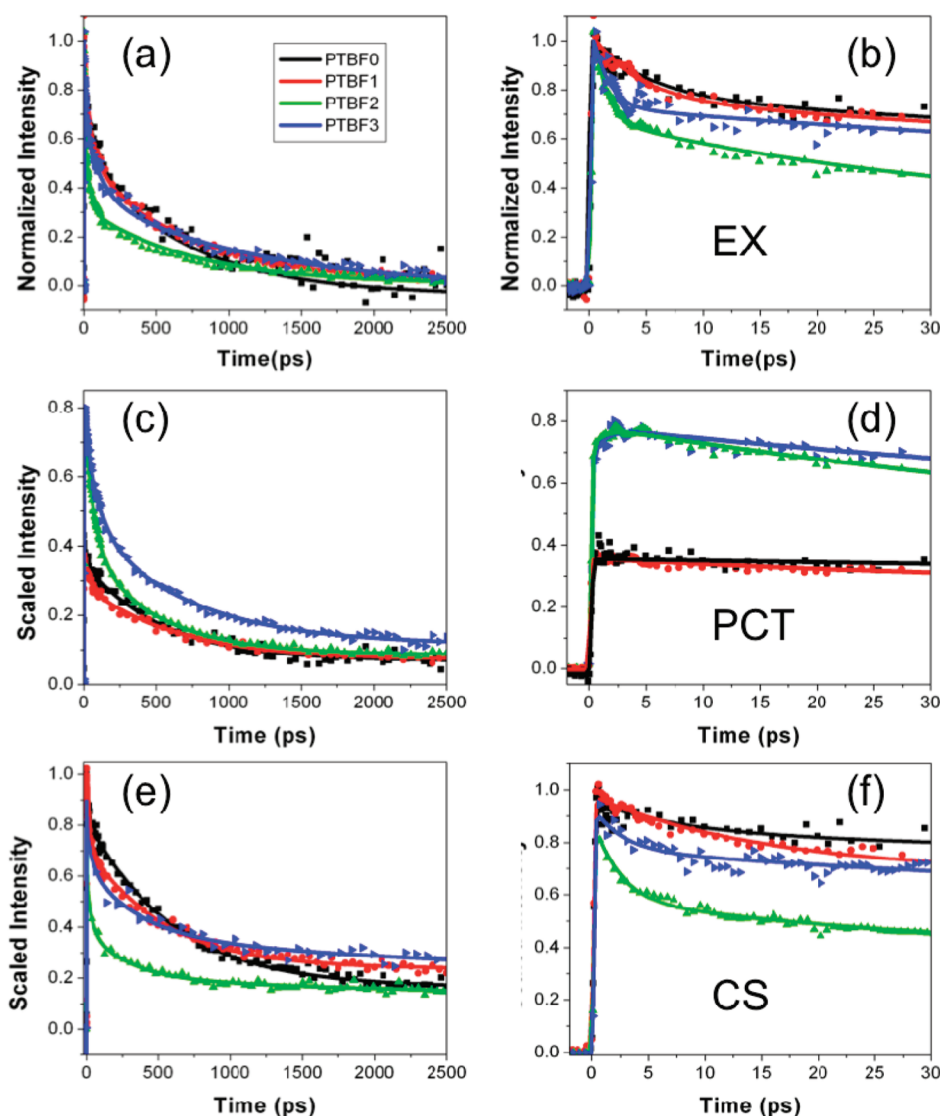


**Figure 7.** Kinetic traces for all transient spectroscopic features under investigation. Figures display 2500 (a, c, e) and 30 ps (b, d, f) of the kinetics. Fits are for EX (a, b), PCT (c, d), and CS (e, f) spectral features.

237 the initial TA spectrum, which resulted in a spectral feature at  
 238 approximately 1350 nm that we assigned as the TA of the EX  
 239 state. The scaling factor was based on the data analysis fits for  
 240 the contributions from the other features, extrapolated to the  
 241 early delay time based on kinetics parameters of other two TA  
 242 features (see the Supporting Information).

243 In initial fits of the TA spectra with two Gaussian functions  
 244 the reconstructed TA spectra did not fit well with the  
 245 experimental data, as shown in the Supporting Information.  
 246 Therefore, a three-Gaussian function fit was used, resulting in  
 247 an almost perfect fit with very little residuals left in the  
 248 difference spectra between the experimental spectra and the  
 249 reconstructed TA spectra (Supporting Information). The three-  
 250 Gaussian function fit of the TA data resulted in three broad  
 251 peaks centered at approximately 1000, 1150, and 1350 nm. The  
 252 additional feature at approximately 1000 nm is tentatively  
 253 assigned to an intramolecular “pseudo”-charge-transfer (PCT)  
 254 state. In this state, the exciton has split into a hole–electron  
 255 pair that is still close enough to experience a Coulombic  
 256 attraction.<sup>19,30</sup> Meanwhile, we also considered other possible  
 257 assignments and subsequently ruled them out for the following

reasons. Triplet states can be ruled out because the formation 258  
 (<1 ps) and decay (largely <1 ns) of this feature are both too 259  
 short for conjugated polymers.<sup>29,31</sup> The polymer anion can be 260  
 ruled out because the decay kinetics of this feature differ 261  
 significantly from that of the cation. In addition, as will be 262  
 discussed subsequently, this feature near 1000 nm also has a 263  
 rise time correlating well with the decay of the EX peak in 264  
 solution, indicating its generation is directly from the EX state. 265  
 Also, blue shifting of the cation spectra has been reported in the 266  
 literature due to counterion stabilization.<sup>32–37</sup> While there is no 267  
 counterion in the TA experiment, the electron itself can act 268  
 similarly to the counterion to stabilize the cation in an 269  
 intramolecular charge-transfer state as long as it is proximal, 270  
 which also fits the description of the PCT. Additionally, this 271  
 transient species has precedence in other alternating copoly- 272  
 mers in the literature.<sup>19,38</sup> 273

On the basis of the above considerations, the time-resolved 274  
 900–1400 nm TA spectra were fit to three Gaussian peaks at 275  
 approximately 1000, 1150, and 1350 nm, whose intensities are 276  
 used to characterize the kinetics of the three Gaussian spectral 277  
 features, assigned to intramolecular pseudo-charge-transfer 278 279

Table 1. Time Constants ( $\tau$ ) and Pre-Exponential Weights ( $A$ ) for EX, PCT, and CS State Transient Absorption Kinetics Fits<sup>a</sup>

sample	state	$\tau_1$ (ps)	$\tau_2$ (ps)	$\tau_3$ (ps)	$\tau_4$ (ps)	$A_1$ (%)	$A_2$ (%)	$A_3$ (%)	$A_4$ (%)
PTBF0	EX	5 (0.9)	99 (25)	700 (43)		23 (1.6)	23 (3.5)	54 (3.8)	
PTBF1	EX	4 (0.3)	87 (8)	800 (24)		25 (0.8)	27 (1.4)	47 (1.5)	
PTBF2	EX	1 (0.1)	31 (1)	730 (16)		40 (0.9)	30 (0.5)	30 (0.4)	
PTBF3	EX	1 (0.1)	100 (7)	1100 (41)		32 (1.3)	32 (1.3)	37 (1.3)	
PTBF0	PCT			525 (20)	>2800			87 (0.9)	13 (0.7)
PTBF1	PCT		40 (5)	632 (27)	>2800		19 (1.2)	60 (1.1)	21 (0.7)
PTBF2	PCT	1 (0.1)	71 (4)	480 (33)	>2800	(rise)	52 (2.4)	41 (2.3)	7 (0.2)
PTBF3	PCT	1 (0.1)	91 (10)	670 (68)	>2800	(rise)	41 (3.7)	50 (3.4)	9 (0.5)
PTBF0	CS	8 (1.1)		590 (14)	>2800			70 (0.5)	17 (0.6)
PTBF1	CS	14(0.7)		518 (13)	>2800			50 (0.5)	25 (0.3)
PTBF2	CS	2 (0.1)	38 (2)	292 (4)	>2800	37 (1.3)	23 (0.4)	25 (0.3)	16 (0.1)
PTBF3	CS	3 (0.5)	53 (4)	377 (6)	>2800	19 (2.1)	17 (0.7)	35 (0.5)	29 (0.1)

<sup>a</sup>Parentheses contain the standard deviation for each fitting parameter.

(PCT), charge-separated (CS), and exciton (EX) states (Figure 6), respectively. The “pseudo” designation distinguishes this intramolecular charge-transfer state from donor:acceptor charge-transfer states that are more typically discussed in the literature. All three states have been characterized previously in other OPV materials by calculations<sup>39–41</sup> and experiments<sup>19,20,42</sup> in the literature.

Figure 7 displays kinetics scaled by the initial population of excitons extracted from global fits of the two-dimensional (time delay  $t$  and wavelength  $\lambda$ ) TA data sets,  $\Delta OD(t, \omega)$ . Each of these kinetics was subsequently fit to a Gaussian function in the energy dimension and multiplied to linear combinations of exponential functions in the delay time dimension with pre-exponential coefficients that reflect the time evolution for the populations of the three species at a particular wavelength. The two-dimensional TA data therefore can be expressed as  $\Delta OD(\omega, t) = \sum_x B_x(\omega) \sum_n A_n^x(\omega) \exp(-t/\tau_n^x)$ , where  $x$  denotes EX, PCT, or CS,  $n$  is the index of the exponential components,  $\tau$  is the time constant,  $t$  is the time delay between the pump and probe pulses, and  $A_n^x(\omega)$  is the weight of the  $n$ th exponential component of transient species  $x$  at the probe energy expressed in wavenumber  $\omega$ . The fitting parameters and their standard deviations are shown in Table 1, and the parameters for  $B(\omega)$  are shown in Table S1 in the Supporting Information.

The EX kinetics (Figure 7a and 7b) of all polymers are best fit by a sum of three exponential components,  $n = 1–3$  (Table 1). The EX-to-PCT and EX-to-CS conversions largely occur within the 160 fs instrument response function time, similar to what was predicted theoretically for a different isolated conjugated polymer, polyphenylenevinylene (PPV).<sup>41</sup> The long decay time constant,  $\tau_3^{\text{EX}} = 700–1100$  ps, is similar to the exciton lifetime in isolated P3HT.<sup>29,43</sup> Hence,  $\tau_3^{\text{EX}}$  in the EX kinetics most likely arises from the excitons that do not undergo the EX-to-PCT or EX-to-CS processes.

The PCT spectral feature (Figure 7c and 7d) is generated within the IRF time in all polymers. However, only PTBF2 and PTBF3 have an additional rise of this feature with a time constant of  $\tau_1^{\text{PCT}} = 1$  ps, which correlated well with a concurrent decay component of the EX signal but not with the ground-state bleach (GSB) signal (Figure S7, the Supporting Information). Hence, this kinetic process is most likely due to an additional slower PCT generation process after the instantaneous process unresolved in our TA setup with a 160 fs IRF (see the Supporting Information). The rise of the PCT population in PTBF2 and PTBF3 is ascribed to intramolecular, geminate hole–electron pair trapping after localized exciton

splitting, which generates the initial EX-to-PCT and EX-to-CS conversion in <160 fs in PTBF0 and PTBF1 (Figure 8).

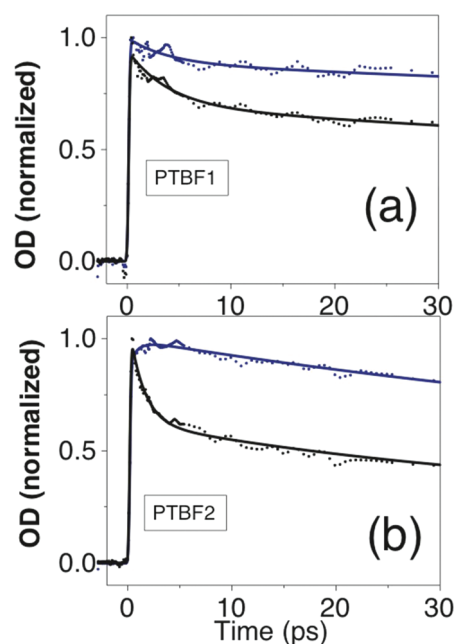


Figure 8. Transient absorption EX (black) and PCT (blue) kinetics for PTBF1 (a) and PTBF2 (b). PTBF2 exhibits a concurrent decay in the EX population and rise in the PCT population, while the PTBF1 population does not.

Intramolecular exciton splitting occurs on a time scale much smaller than 100 fs, as calculated by Bedard-Hearn et al.<sup>41</sup> Therefore,  $\tau_1^{\text{PCT}}$  is too long to account for ultrafast exciton delocalization generally on the time scale of  $\sim 100$  fs.<sup>41</sup> Due to their lifetimes,<sup>19</sup> the two other decay time constants of the PCT feature,  $\tau_2^{\text{PCT}}$  and  $\tau_3^{\text{PCT}}$ , are assigned, respectively, to intrachain geminate recombination and interchain recombination of charge carriers occurring across self-aggregated polymer fragments of a single polymer (Figure 6).

The CS kinetics (Figure 7e and 7f) were obtained by the spectral signal of the polymer cation. As opposed to BHJ film kinetics, the entire cation population in isolated polymers in solution is generated within 160 fs after photoexcitation. Subsequently, the shortest decay time constant  $\tau_1^{\text{CS}}$  is 2–3 ps for PTBF2 and PTBF3 and 8–13 ps for PTBF0 and PTBF1. PTBF2 and PTBF3 also exhibit an additional decay channel

343  $\tau_2^{\text{CS}}$  at 21 (24%) and 98 ps (23%), respectively. The time  
344 constant  $\tau_3^{\text{CS}}$  is 270–650 ps and has a larger pre-exponential  
345 weight as the number of fluorine atoms decreases.

## 4. DISCUSSION

346 **4.1. Influence of Polymer Local Electronic Structures**  
347 **on Exciton and Charge-Separation Dynamics.** One major  
348 consideration for achieving a high PCE in OPV devices is  
349 overcoming the exciton binding energy in order to achieve  
350 efficient charge separation.<sup>44</sup> This challenge is typically  
351 addressed using a BHJ architecture and relying on the  
352 LUMO energy offset between the donor polymer and the  
353 acceptor (e.g., PCBM) at their interface to split the  
354 exciton.<sup>26,45,46</sup> This LUMO energy offset requirement of  
355  $\sim 0.3$ – $0.5$  eV approximates the exciton splitting driving force  
356 based on the Marcus–Hush model<sup>47</sup> and assumes that the  
357 lowest energy electronic transition is almost entirely a  
358 HOMO–LUMO transition of the donor polymer.<sup>48</sup> However,  
359 this current picture ignores structural details at the donor–  
360 acceptor interfaces as well as the local field effects by charged  
361 species which could significantly alter the redox potentials and  
362 energies of relevant states.<sup>23</sup> Moreover, alternating copolymers  
363 deviate from the trend between charge-separation driving force  
364 and geminate recombination efficiency, which has been found  
365 for several homopolymer OPV materials (e.g., P3HT).<sup>23,49</sup> For  
366 example, some alternating copolymers exhibit a lower driving  
367 force of 0.1–0.2 eV required for achieving low geminate  
368 recombination and high cation populations, such as  
369 PCPDTBT.<sup>21</sup> These exceptions suggest the importance of  
370 intramolecular local structural details in estimating energetic  
371 costs for exciton splitting in alternating copolymers, such as the  
372 relative distance and orientation of the donor and acceptor at  
373 the domain interface in the BHJ films as well as the intrinsic  
374 electronic structures of the alternating blocks along the polymer  
375 chain.

376 As discussed earlier, the electron affinity of TT is higher than  
377 that of BDT in the PTBF polymer series, which establishes a  
378 local electron density gradient along the polymer backbone.  
379 Additional electron-withdrawing fluorine atoms will further  
380 modulate the electron density distribution in the ground and  
381 excited states. For example, adding a fluorine atom at the X<sub>1</sub>  
382 position on TT to form PTBF1 (Figure 1) will enhance the  
383 electron-pulling effect toward TT, resulting in higher local  
384 charge-transfer character. In comparison, adding fluorine atoms  
385 at two X<sub>2</sub> positions in BDT instead at the X<sub>1</sub> position to form  
386 PTBF2 will pull the electron density in an opposite direction,  
387 away from TT, and partially negate the electron-withdrawing  
388 direction established in PTBF1. Furthermore, adding three  
389 fluorine atoms at X<sub>1</sub> and X<sub>2</sub> to form PTBF3 will again pull the  
390 electron slightly toward TT compared to that in PTBF2. These  
391 “push–pull” actions on the electron density are reflected in the  
392 magnitudes of local electronic dipole moments in the  
393 monomers of all four polymers in an order of PTBF1 >  
394 PTBF0 > PTBF3 > PTBF2 (Supporting Information) and  
395 cause subtle yet important differences in the intramolecular  
396 exciton splitting dynamics and relative populations of the  
397 transient species in the PTBF as well as other polymers.<sup>26,50</sup> As  
398 shown in previous work,<sup>1,26</sup> such chemical modifications also  
399 influence the device performance significantly. Here, we intend  
400 to rationalize the effects by differences in the local electronic  
401 structures of the polymer chain and their implications for  
402 device performance.

Our studies have revealed that isolated PTBF polymers *alone* 403  
are capable of intramolecular charge transfer between adjacent 404  
polymer moieties, but their exciton dynamics and initial relative 405  
populations of EX, PCT, and CS states vary. In order to 406  
understand these results, we first need to know what the 407  
equivalent electron donor and acceptor are in isolated 408  
copolymers and what drives intramolecular charge separation 409  
in the absence of external electron acceptor. 410

In isolated conjugated homopolymers such as P3HT, exciton 411  
splitting originates from the localization of an initially 412  
delocalized exciton to form a polaron, driven by nuclear 413  
reorganization upon a shift in charge density, and consequent 414  
formation of a Coulombically bound, closely located electron– 415  
hole pair.<sup>51</sup> This suggests that exciton splitting is facilitated by a 416  
local asymmetry of electron density or charge gradients in 417  
combination with the structural reorganization that results in a 418  
potential energy barrier to prevent geminate recombination. 419  
Because of the built in local electron density gradient along the 420  
polymer backbone, the initial exciton splitting mechanism will 421  
be significantly different in alternating copolymers. Compre- 422  
hensive calculations by Risko, McGehee, and Brédas on the 423  
electronic structures of several oligomer models corresponding 424  
to alternating copolymers showed that the first excited state S<sub>1</sub> 425  
was dominated by the HOMO–LUMO transition (>90%), 426  
accompanied by significant electron density displacement along 427  
the polymer backbone.<sup>52</sup> Such an electron density displacement 428  
in the exciton was also seen in our calculations in the model 429  
tetramers (Figure 3), implying that a “hole”-like electron 430  
density depletion is produced in one segment while an 431  
“electron”-like electron density enrichment is simultaneously 432  
generated in another segment of the polymer, resulting in a 433  
polarized exciton. 434

Because isolated polymer chains in solution are known to 435  
have C–C bond twists, resulting in  $\pi$ -conjugation disruptions 436  
and local structural variations or defects, it is difficult to identify 437  
accurately the electron donor and acceptor segments in these 438  
isolated polymers as shown in Figures 3 and 6. Moreover, the 439  
size of the exciton, a range of the effective displacement of the 440  
electron density from HOMO to LUMO, is unclear from 441  
calculations with a limited length of the backbone. Although 442  
large-scale computations combining molecular dynamics 443  
simulation with quantum mechanical theory may verify this 444  
proposed intramolecular electron donor–acceptor model, such 445  
calculations are beyond the scope of the current work. 446  
Nevertheless, the calculated results of HOMO–LUMO 447  
electron density distributions (BDT–TT)<sub>4</sub> and TT–(BDT– 448  
TT)<sub>4</sub> oligomers (Figure 3) provide a basis for a segmented 449  
donor and acceptor model due to the electron gradient across 450  
the polymer chain. 451

The above model suggests a possible general mechanism for 452  
intramolecular charge separation in the alternating polymers, 453  
while different exciton-splitting dynamic behaviors among the 454  
four PTBF polymers need to be further explained in terms of 455  
fine tuning the electronic structures by the pendant fluorine 456  
atoms. The order of magnitude of the dipole moment change 457  
 $\Delta\mu_{\text{eg}}$  (i.e.,  $\mu_{\text{ex}} - \mu_{\text{gs}}$ ) in monomers via a HOMO–LUMO 458  
transition suggests that PTBF1 could potentially have the most 459  
polarized exciton, with the largest effective electron–hole 460  
displacement compared to the excitons of other polymers in 461  
this series. Consequently, PTBF1 has the highest relative CS/ 462  
PCT population as well as the highest PCE from our previous 463  
studies.<sup>26</sup> In contrast, PTBF2 has the smallest  $\Delta\mu_{\text{eg}}$  upon the 464  
HOMO–LUMO transition and the highest initial PCT 465

466 population, which lead to geminate recombination of the hole  
467 and electron. Evidently, a larger local  $\Delta\mu_{eg}$  facilitates a better  
468 hole–electron separation in the exciton state, implying this  
469 more polarized exciton makes charge separation easier. In  
470 contrast, the smallest dipole change in the monomer of **PTBF2**  
471 is due to the electron density being pulled in opposite  
472 directions by two electron-withdrawing sources, fluorine atoms  
473 on **TT** and **BDT** units. Apparently, for exciton splitting in  
474 conjugated polymers, a larger local dipole change is desirable,  
475 which can be rationalized by a larger resulting hole and electron  
476 distance to weaken the attractive Coulombic interactions.

477 Besides the intrinsic local dipole moment change in these  
478 polymers, the energy difference between the EX and the CS or  
479 PCT states needs to be considered in the EX-to-PCT and EX-  
480 to-CS processes. As an exciton splits, the resulting hole–  
481 electron separation could initially have different separation  
482 distances according to the excess energy and local environment.  
483 A larger  $\Delta\mu_{eg}$  facilitates the EX-to-CS process with resulting  
484 large hole–electron separation distances, while a smaller  $\Delta\mu_{eg}$   
485 stabilizes strongly interacting hole–electron pairs in the PCT  
486 state at a lower energy than the CS state (Figure 9). **PTBF2**

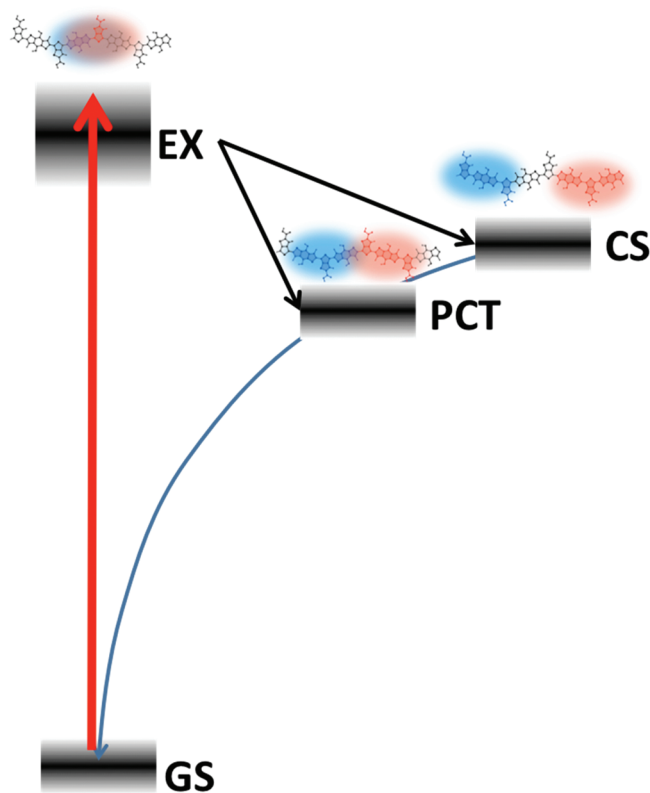


**Figure 9.** Schematic illustration of the states and pathways involved in the early exciton splitting dynamics of the isolated **PTBF** polymers in solution. Fuzzy energy levels describe the energy dispersion due to the structural inhomogeneity in isolated polymers in solution. Holes are indicated with a blue region on the polymer backbone, while electrons are indicated in red. Size of these regions provides a qualitative description of the hole and electron delocalization only. Curved downward arrow follows the potential energy as a function of the hole–electron separation as approximated in the Onsager model as well as the direction of the recombination for the CS and PCT states. GS denotes the ground state.

487 and **PTBF3** polymers with smaller monomer  $\Delta\mu_{eg}$  not only  
488 have the higher PCT population within the IRF time but also

show additional formation of PCT for the EX-to-PCT 489  
conversion during EX localization. In contrast, **PTBF0** and 490  
**PTBF1**, with larger  $\Delta\mu_{eg}$  values in the polymer fragments, favor 491  
EX-to-CS conversion processes and are only able to undergo 492  
the EX-to-PCT transition in <160 fs, when the excitons may 493  
not yet have been as strongly confined by nuclear motions.<sup>51</sup> In 494  
both cases, the “push–pull” character in these polymers has 495  
defrayed a part of the cost for exciton splitting to produce the 496  
CS and PCT states. If an external acceptor is in the proximity to 497  
the electron density-rich segment in the backbone, forming a 498  
“donor–acceptor1–acceptor2 triad”, it can take the electron 499  
that has already been intramolecularly separated from the hole, 500  
reducing the required exciton splitting driving force. 501

#### 4.2. Branched Pathways from Exciton to Charge

**Separation.** A simplified energy diagram with dynamic 502  
pathways is proposed for intramolecular processes (Figure 9). 503  
Local conformational variation in the polymers results in 504  
energy variation of the three states; hence, the TA features of 505  
these states are inhomogeneously broadened. The PCT state 507  
has a lower potential energy than the CS state because the 508  
separated, yet closely positioned, hole–electron pairs experi- 509  
ence an attractive Coulombic interaction that stabilizes the 510  
PCT state.<sup>23</sup> Different polarities due to the intrinsic dipole 511  
change of the polymer or the surroundings will affect the local 512  
dielectric constant and exciton polarization and hence the initial 513  
hole–electron separation distance. 514

This model agrees with our experimental observation, where 515  
the EX-to-PCT conversion is prominent in **PTBF2** and **PTBF3** 516  
while the EX-to-CS process dominates in **PTBF1** and **PTBF0**. 517  
Because the PCT state on average has shorter hole–electron 518  
separation, the former two polymers are more in favor of 519  
trapping for the strongly bound electron–hole pair originated 520  
from intramolecular exciton splitting. In reality, the trans- 521  
formation from EX to PCT and CS could coexist depending on 522  
local structure. Here, we suggested branched pathways of EX- 523  
to-CS and EX-to-PCT that could coexist and the different 524  
**PTBF** polymers (Figure 9), according to their electronic 525  
structures and polarity of the exciton, could have their 526  
preferences. 527

#### 4.3. Influence of the Branched Exciton Pathways on

**Device Performances.** To determine the importance of 528  
branching ratio for intrachain exciton splitting from EX to PCT 529  
or CS, we defined a parameter named the *relative branching* 530  
ratio (RBR) that is the ratio of the two amplitude coefficients 531  
 $A_{CS}/A_{PCT}$  at the time after photoexcitation when the PCT 532  
signal is maximized. Note that the RBR does not give an exact 533  
ratio of the CS and PCT populations because the extinction 534  
coefficients for these states are not necessarily equal, while the 535  
extinction coefficients for the same species are assumed to be 536  
the same across the four polymers. To our surprise, linear 537  
correlations between the RBR of the isolated polymer *in* 538  
*solution* and the PCE and FF of the BHJ *devices* made from 539  
these polymers<sup>26</sup> appear with good fidelity ( $r^2 = 0.91$  or  $0.97$ , 540  
respectively) (Figure 10), even though potentially important 541  
factors for the BHJ performance (e.g., polymer packing or 542  
donor:acceptor potential energy offsets) are absent. However, 543  
only a poor correlation of RBR and device  $V_{oc}$  was observed in 544  
the **PTBF** polymer series.<sup>24,25</sup> While the cause of such 545  
correlations is not fully understood, such intramolecular RBR 546  
and BHJ device PCE connections have not been observed 547  
previously. This correlation emphasizes that a molecular 548  
picture, with a focus on local intramolecular interactions 549  
instead of the commonly used energy band model, is more 550  
551

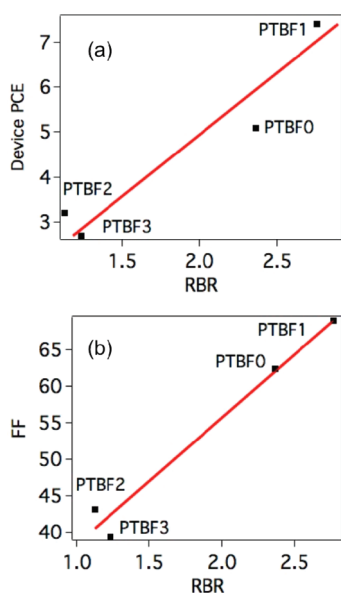


**Figure 10.** Relative branching ratios (RBR) of CS/PCT populations for polymer solutions versus OPV device PCE (a) and FF (b).

552 important than we previously thought in OPV applications  
 553 using these low-band-gap polymers with charge-transfer  
 554 character. This observation therefore carries implications in  
 555 future OPV polymer design, where not only the position of the  
 556 donor and acceptor energy levels but also the local structure  
 557 facilitates that splitting excitons needs to be considered.

558 A linear relationship between solution RBR and device PCE  
 559 or FF also implies that CS and PCT states in isolated charge-  
 560 transfer copolymers could be precursors for or closely related to  
 561 the CS and trapped CT states in the BHJ films. Because most  
 562 of the intramolecular EX-to-CS and EX-to-PCT processes  
 563 occur in  $<160$  fs in these polymers, the relative populations of  
 564 CS and PCT have been established before the intermolecular  
 565 charge transfer to PCBM in BHJs.<sup>10</sup> Therefore, the CS state  
 566 population is proportional to the free charge carrier  
 567 populations, while the trapped PCT state population leads to  
 568 the geminate recombination. When the intramolecular CS takes  
 569 place, it preseparates hole and electron pairs and hence defrays  
 570 a part of the cost for charge separation between the donor  
 571 copolymer and PCBM. This makes it less energetically  
 572 expensive for an acceptor to subsequently extract the electron,  
 573 because that acceptor no longer pays the full cost of  
 574 counteracting the Coulombic hole–electron attraction of an  
 575 exciton. Hence, the polymer’s intramolecular CS state  
 576 population is energetically favorable for external electron  
 577 acceptors to extract electrons from the polymer due to its  
 578 relatively weak Coulombic attraction between electrons and  
 579 holes. In comparison, the energetic cost for an external electron  
 580 acceptor to extract an electron from the polymer’s PCT state is  
 581 higher due to a stronger Coulombic attraction between the  
 582 hole–electron pair. On the basis of the a good correlation  
 583 between RBR and FF in this series, fine tuning the “push–pull”  
 584 interaction between neighboring monomers such that the CS/  
 585 PCT population ratio is maximized is a promising method to  
 586 optimize PCE and FF and potentially could be performed  
 587 simultaneously to  $V_{oc}$  optimization. Our results also point out  
 588 that an increase in the exciton polarity would enhance the CS  
 589 state population and even the device PCE or FF, but this

hypothesis will be further investigated through new materials in  
 our future studies.

**4.4. Implications of the “Defrayed Energetic Cost” in  
 OPV Polymer Design.** As new and more complex polymers  
 are synthesized for OPV applications, the contemporary  
 organic semiconductor picture for conjugated polymers needs  
 to be revised for the alternating “push–pull” copolymers where  
 localized, ultrafast, molecule-like behaviors could play impor-  
 tant roles in the OPV functions and even in photovoltaic  
 devices. In the process of improving the device PCE through  
 chemical tuning one needs to consider a balance between  
 factors which may not be fully appreciated. This balance is  
 between harnessing the optimal driving force to generate free  
 carriers from excitons and generating Coulombically trapped  
 charge carriers that are more difficult for the acceptor to extract.  
 The former would lead to more efficient charge extraction in an  
 OPV device, while the latter would lead to less. Therefore, the  
 intramolecular PCT kinetics discussed here suggest a need to  
 rethink charge pair trapping and exciton splitting for alternating  
 copolymers based on the electronegativity and position of the  
 backbone’s pendant moieties, because these events are usually  
 considered to be intermolecular, occurring at the donor:-  
 acceptor boundary of BHJs, but our results show that actually  
 the intramolecular processes are also significant. Designing  
 polymers that induce these events in an optimal ratio may lead  
 to improved device efficiency, especially if future polymers can  
 be tuned to preferentially generate CS population intra-  
 molecularly. Further research must be done to understand  
 the losses associated with inducing these intramolecular charge  
 traps and driving forces, the extent to which they can be  
 optimized.

## 5. CONCLUSION

We addressed the significance of intramolecular pseudo-charge-  
 transfer (PCT) and charge-separated (CS) states in four  
 polymers of the PTBF species in solution. Our studies indicate  
 that polymer modifications by fluorination tune the energy  
 levels of the polymers with respect to the intramolecular PCT  
 and CS states, which leads to a delicate balance in populating  
 the CS or PCT states and to two possible outcomes in the  
 intramolecular transient population, desirable charge separation  
 or undesirable charge trapping. Finally, the dependence of these  
 states on solar device efficiency was also highlighted. These  
 findings suggest a systematic method to modulate the extent of  
 intramolecular charge separation or pseudo-charge transfer in  
 alternating copolymers, and their surprisingly well-correlated  
 relationship to device performance has been brought to the  
 OPV community’s attention in designing alternating “donor–  
 acceptor” copolymer systems. Our study reveals the origin of  
 such a connection and suggests that these copolymers distinctly  
 differ from previously studied homopolymers because of their  
 local molecule-like nature that may play important roles in  
 device performance. The intramolecular exciton separation  
 driving force suggests the presence of a charge-separating  
 “triad” by two hole-rich and electron-rich segments along the  
 polymer backbone with the external electron acceptor PCBM  
 at the BHJs, to facilitate charge transfer with less geminate  
 recombination, as well as to hinder the geminate recombina-  
 tion. The details of these two outcomes in BHJ films, the nature  
 of the RBR and device parameter correlations, will be discussed  
 in our future reports.

## 649 ■ ASSOCIATED CONTENT

## 650 ● Supporting Information

651 Discussion of sample conditions, fitting protocol for transient  
652 absorption data, ground-state bleach comparison, conditions for  
653 reduction of exciton–exciton annihilation signal, oxidized  
654 polymer steady-state absorption, and dipole monomer  
655 calculations. This material is available free of charge via the  
656 Internet at <http://pubs.acs.org>.

## 657 ■ AUTHOR INFORMATION

## 658 Corresponding Author

659 E-mail: [lchen@anl.gov](mailto:lchen@anl.gov); [lupingyu@uchicago.edu](mailto:lupingyu@uchicago.edu)

## 660 Notes

661 The authors declare no competing financial interest.

## 662 ■ ACKNOWLEDGMENTS

663 This research was supported by the ANSER Center, an Energy  
664 Frontier Research Center funded by the U.S. Department of  
665 Energy, Office of Science, Office of Basic Energy Sciences,  
666 under Award Number DE-SC0001059. Part of the equipment  
667 and laboratory setting was supported by the Division of  
668 Chemical Sciences, Office of Basic Energy Sciences, the U.S.  
669 Department of Energy under contract DE-AC02-06CH11357  
670 (for L.X.C.). The gift from Intel Corp. to L.X.C. and L.Y. is  
671 greatly appreciated for a part of research related to film  
672 fabrication. We also thank Drs. David J. Gosztola and Gary  
673 Wiederrecht for their help in the Center for Nanoscale  
674 Materials at Argonne National Laboratory. Use of the facilities  
675 at the Center for Nanoscale Materials was supported by the  
676 U.S. Department of Energy, Office of Science, Office of Basic  
677 Energy Sciences, under Contract No. DE-AC02-06CH11357.

## 678 ■ REFERENCES

- 679 (1) Liang, Y.; Xu, Z.; Xia, J.; Tsai, S.-T.; Wu, Y.; Li, G.; Ray, C.; Yu, L.  
680 *Adv. Mater.* **2010**, *22*, E135.  
681 (2) He, Z.; Zhong, C.; Huang, X.; Wong, W.-Y.; Wu, H.; Chen, L.;  
682 Su, S.; Cao, Y. *Adv. Mater.* **2011**, *23*, 4636.  
683 (3) Chen, H.-Y.; Hou, J.; Zhang, S.; Liang, Y.; Yang, G.; Yang, Y.; Yu,  
684 L.; Wu, Y.; Li, G. *Nat. Photonics* **2009**, *3*, 649.  
685 (4) Korovyanko, O. J.; Österbacka, R.; Jiang, X. M.; Vardeny, Z. V.;  
686 Janssen, R. A. J. *Phys. Rev. B* **2001**, *64*, 235122.  
687 (5) Szarko, J. M.; Rolczynski, B. S.; Guo, J.; Liang, Y.; He, F.; Mara,  
688 M. W.; Yu, L.; Chen, L. X. *J. Phys. Chem. B* **2010**, *114*, 14505.  
689 (6) Schwartz, B. J. *Annu. Rev. Phys. Chem.* **2003**, *54*, 141.  
690 (7) Pingree, L. S. C.; Reid, O. G.; Ginger, D. S. *Adv. Mater.* **2009**, *21*,  
691 19.  
692 (8) Rance, W. L.; Ferguson, A. J.; McCarthy-Ward, T.; Heeney, M.;  
693 Ginley, D. S.; Olson, D. C.; Rumbles, G.; Kopidakis, N. *ACS Nano*  
694 **2011**, *5*, 5635.  
695 (9) Joshi, S.; Grigorian, S.; Pietsch, U. *Phys. Status Solidi A* **2008**, *205*,  
696 488.  
697 (10) Guo, J.; Liang, Y.; Szarko, J.; Lee, B.; Son, H. J.; Rolczynski, B.  
698 S.; Yu, L.; Chen, L. X. *J. Phys. Chem. B* **2010**, *114*, 742.  
699 (11) Szarko, J. M.; Guo, J.; Liang, Y.; Lee, B.; Rolczynski, B. S.;  
700 Strzalka, J.; Xu, T.; Loser, S.; Marks, T. J.; Yu, L.; Chen, L. X. *Adv.*  
701 *Mater.* **2010**, *22*, 5468.  
702 (12) Siringhaus, H.; Brown, P. J.; Friend, R. H.; Nielson, M. M.;  
703 Bechgaard, K.; Langeveld-Voss, B. M. W.; Spiering, A. J. H.; Janssen, R.  
704 A. J.; Meijer, E. W.; Herwig, P.; Leeuw, D. M. d. *Nature* **1999**, *401*,  
705 685.  
706 (13) Dante, M.; Peet, J.; Nguyen, T. *J. Phys. Chem. C* **2008**, *112*,  
707 7241.  
708 (14) Coffey, D. C.; Ferguson, A. J.; Kopidakis, N.; Rumbles, G. *ACS*  
709 *Nano* **2010**, *4*, 5437.  
710 (15) Lewis, N. S. *Science* **2007**, *315*, 798.

- (16) Ma, W.; Yang, C.; Gong, X.; Lee, K.; Heeger, A. J. *Adv. Funct.*  
*Mater.* **2005**, *15*, 1617. 711  
712  
(17) Dante, M.; Garcia, A.; Nguyen, T.-Q. *J. Phys. Chem. C* **2009**,  
*113*, 1596. 713  
714  
(18) Liang, Y.; Feng, D.; Wu, Y.; Tsai, S.-T.; Li, G.; Ray, C.; Yu, L. *J.*  
*Am. Chem. Soc.* **2009**, *131*, 7792. 715  
716  
(19) Westerling, M.; Aarnio, H.; Österbacka, R.; Stubb, H.; King, S.;  
717 Monkman, A.; Andersson, M.; Jespersen, K.; Kesti, T.; Yartsev, A.;  
718 Sundström, V. *Phys. Rev. B* **2007**, *75*, 224306. 719  
(20) Pacios, R.; Nelson, J.; Bradley, D. D. C.; Virgili, T.; Lanzani, G.;  
720 Brabec, C. J. *J. Phys.: Condens. Matter* **2004**, *16*, 8105. 721  
(21) Clarke, T.; Ballantyne, A.; Jamieson, F.; Brabec, C.; Nelson, J.;  
722 Durrant, J. *Chem. Commun.* **2009**, *1*, 89. 723  
(22) Peet, J.; Kim, J. Y.; Coates, N. E.; Ma, W. L.; Moses, D.; Heeger,  
724 A. J.; Bazan, G. C. *Nat. Mater.* **2007**, *6*, 497. 725  
(23) Clarke, T. M.; Durrant, J. R. *Chem. Rev.* **2010**, *32*. 726  
(24) Servaites, J. D.; Ratner, M. A.; Marks, T. J. *Appl. Phys. Lett.* **2009**,  
727 *95*, 163302. 728  
(25) Servaites, J. D.; Yeganeh, S.; Marks, T. J.; Ratner, M. A. *Adv.*  
*Funct. Mater.* **2010**, *20*, 97. 729  
730  
(26) Son, H. J.; Wang, W.; Xu, T.; Liang, Y.; Wu, Y.; Li, G.; Yu, L. *J.*  
*Am. Chem. Soc.* **2011**, *133*, 1885. 731  
732  
(27) Hains, A.; Martinson, A. B. F.; Irwin, M. D.; Yan, H.; Marks, T.  
733 *Polym. Mater.* **2007**, *96*, 814. 734  
(28) Lockard, J. V.; Wasielewski, M. R. *Phys. Chem. B Lett.* **2007**, *111*,  
735 11638. 736  
(29) Guo, J.; Ohkita, H.; Bente, H.; Ito, S. *J. Am. Chem. Soc.* **2009**,  
737 *131*, 16869. 738  
(30) King, S. M.; Hintschich, S. I.; Dai, D.; Rothe, C.; Monkman, A.  
739 *P. J. Phys. Chem. C* **2007**, *111*, 18759. 740  
(31) Carmichael, I.; Hug, G. J. *Phys. Chem. Ref. Data* **1986**, *15*, 1. 741  
(32) Seki, H. *Faraday Trans.* **1992**, *88*, 35. 742  
(33) Langan, J. R.; Salmon, G. A. *J. Chem. Soc., Faraday Trans. 1*  
743 **1982**, *78*, 3645. 744  
(34) Yamamoto, Y.; Aoyama, T.; Hayashi, K. *J. Chem. Soc., Faraday*  
*Trans. 1* **1988**, *84*, 2209. 745  
746  
(35) Yamamoto, Y.; Nishida, S.; Ma, X.-H.; Hayashi, K. *J. Phys. Chem.*  
747 **1986**, *90*, 1921. 748  
(36) Gersdorf, J.; Mattay, J.; Gorner, H. *J. Am. Chem. Soc.* **1987**, *109*,  
749 1203. 750  
(37) Garcia, A.; Brzezinski, J. Z.; Nguyen, T.-Q. *J. Phys. Chem. C*  
751 **2009**, *113*, 2950. 752  
(38) King, S. M.; Hintschich, S. I.; Dai, D.; Rothe, C.; Monkman, A.  
753 *P. J. Phys. Chem. C* **2007**, *111*, 18759. 754  
(39) Beljonne, D.; Shuai, Z.; Pourtois, G.; Bredas, J. L. *J. Phys. Chem.*  
755 *A* **2001**, *105*, 9. 756  
(40) Sterpone, F.; Bedard-Hearn, M. J.; Rossky, P. J. *J. Phys. Chem.*  
757 *Letts. A* **2009**, *113*, 3427. 758  
(41) Bedard-Hearn, M. J.; Sterpone, F.; Rossky, P. J. *J. Phys. Chem. A*  
759 **2010**, *114*, 7661. 760  
(42) Gelinas, S.; Pare-Labrosse, O.; Brosseau, C.-N.; Albert-Seifried,  
761 S.; McNeill, C. R.; Kirov, K. R.; Howard, I. A.; Leonelli, R.; Friend, R.  
762 H.; Silva, C. *J. Phys. Chem. C* **2011**, *115*, 7114. 763  
(43) Hwang, I.; Moses, D.; Heeger, A. J. *Phys. Chem. C* **2008**, *112*,  
764 4350. 765  
(44) Pensack, R. D.; Banyas, K. M.; Barbour, L. W.; Hegadorn, M.;  
766 Asbury, J. B. *Phys. Chem. Chem. Phys.* **2009**, *11*, 2575. 767  
(45) Howard, I. A.; Mauer, R.; Meister, M.; Laquai, F. d. r. *J. Am.*  
768 *Chem. Soc.* **2010**, *132*, 14866. 769  
(46) Barbara, P. F.; Meyer, T. J.; Ratner, M. A. *J. Phys. Chem.* **1996**,  
770 *100*, 13148. 771  
(47) Marcus, R. A.; Sutin, N. *Biochim. Biophys. Acta* **1985**, *811*, 265. 772  
(48) Scharber, M. C.; Mühlbacher, D.; Koppe, M.; Denk, P.;  
773 Waldauf, C.; Heeger, A.; Brabec, C. *Adv. Mater.* **2006**, *78*, 789. 774  
(49) Ohkita, H.; Cook, S.; Astuti, Y.; Duffy, W.; Tierney, S.; Zhang,  
775 W.; Heeney, M.; McCulloch, I.; Nelson, J.; Bradley, D. D. C.; Durrant,  
776 J. J. *Am. Chem. Soc.* **2008**, *130*, 3030. 777

- 778 (50) Carsten, B.; Szarko, J. M.; Son, H.-J.; Wang, W.; Lu, L.; He, F.;  
779 Rolczynski, B. S.; Lou, S. J.; Chen, L. X.; Yu, L. *J. Am. Chem. Soc.* **2011**,  
780 *133*, 20468.
- 781 (51) Beenken, W. J. D.; Pullerits, T. J. *Phys. Chem. B* **2004**, *108*, 6164.
- 782 (52) Risko, C.; McGehee, M. D.; Brédas, J.-L. *Chem. Sci.* **2011**, *2*,  
783 1200.
- 784 (53) Dias, F. B.; Pollock, S.; Hedley, G.; Palsson, L.-O.; Monkman,  
785 A.; Perepichka, I. I.; Perepichka, I. F.; Tavasli, M.; Bryce, M. R. *J. Phys.*  
786 *Chem. B* **2006**, *110*, 19329.